Biodegradable Amphiphilic Copolymer Containing Nucleobase: Synthesis, Self-Assembly in Aqueous Solutions, and Potential Use in Controlled Drug Delivery

ARTICLE *in* BIOMACROMOLECULES · AUGUST 2012

Impact Factor: 5.75 · DOI: 10.1021/bm301169x · Source: PubMed

6 AUTHORS, INCLUDING:

Suhong Wu
Houston Methodist Leading Medicine
13 PUBLICATIONS **122** CITATIONS
SEE PROFILE

Zhigang Xie
Chinese Academy of Sciences
135 PUBLICATIONS **3,373** CITATIONS
SEE PROFILE

Yubin Huang
Chinese Academy of Sciences
146 PUBLICATIONS **1,525** CITATIONS
SEE PROFILE

Article

pubs.acs.org/Biomac

Biodegradable Amphiphilic Copolymer Containing Nucleobase: Synthesis, Self-Assembly in Aqueous Solutions, and Potential Use in Controlled Drug Delivery

Huihui Kuang,[†,‡] Suhong Wu,[†,‡] Zhigang Xie,[†] Fanbo Meng,[*,§] Xiabin Jing,[†] and Yubin Huang[*,†]

[†]State Key Laboratory of Polymer Physics and Chemistry, Changchun Institute of Applied Chemistry, Chinese Academy of Sciences, Changchun 130022, P. R. China

[‡]Graduate School of Chinese Academy of Sciences, Beijing 100039, P. R. China

[§]The Cardiology Department of China-Japan Union Hospital of Jilin University, No. 126 Xiantai Str., Changchun 130033, P. R. China

Supporting Information

ABSTRACT: Biodegradable nucleobase-grafted amphiphilic copolymer, the methoxyl poly (ethylene glycol)-*b*-poly (L-lactide-*co*-2-methyl-2(3-(2,3-dihydroxylpropylthio) propyloxy-carbonyl)-propylene carbonate/1-carboxymethylthymine) (mPEG-*b*- P(LA-*co*-MPT)), was synthesized. ^{1}H NMR titration and FT-IR spectroscopy indicated that the hydrogen-bonding could be formed between mPEG-*b*-P(LA-*co*-MPT) and 9-hexadecyladenine (A-C16). The hydrophobic microenvironment of the amphiphilic copolymer can protect the complementary multiple hydrogen bonds between mPEG-*b*-P(LA-*co*-MPT) and A-C16 from water effectively. The addition of A-C16 not only lowered the critical aggregation concentration (CAC) of mPEG-*b*-P(LA-*co*-MPT)/A-C16 nanoparticles (NPs) in aqueous solution but also induced different morphologies, which can be observed by transmission electron microscopy (TEM). Meanwhile, dynamic light scattering (DLS) and turbidometry was utilized to evaluate the effect of temperature and pH change on the stability of mPEG-*b*-P(LA-*co*-MPT)/A-C16 NPs. Cytotoxicity evaluation showed good biocompatibility of the mPEG-*b*-P(LA-*co*-MPT)/A-C16 NPs. The *in vitro* drug release profile showed that with the increase of A-C16 content, the doxorubiucin (DOX) release at pH 7.4 decreased, while the faster release rate was observed with the addition of A-C16 with a pH of 5.0. Importantly, DOX-loaded NPs exerted comparable cytotoxicity against MDA-MB-231 cells. This work provided a new method to stabilize NP structure using hydrogen-bonds and would have the potential to be applied in controlled drug delivery.

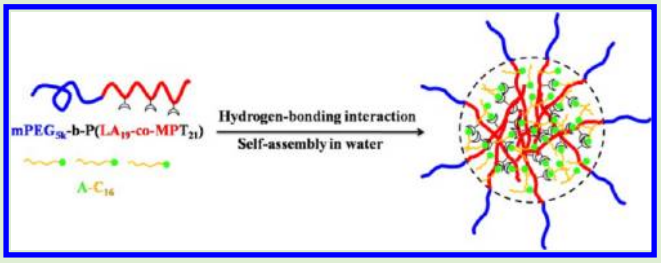

INTRODUCTION

A noncovalent bond is widely used in the preparation of various molecular architectures in the past decades because of its dynamic response to the assemblies.[1] In addition, hydrogen-bond-mediated noncovalent bonds are very attractive because they are highly directional and sometimes give strong binding when multiple hydrogen-bonds are formed together.[2] Especially in 1953, James Watson and Francis Crick expounded the importance of the complementary adenine−thymine (A−T) and guanine−cytosine (G−C) base-pairing in the structure of the DNA double helix.[3] Scientists also found that base-pairs played an important role in biological information storage, genetic coding, and protein synthesis.[4] Then chemists began to investigate the hydrogen bonding between the nucleobases and to utilize such highly specific interactions to design drugs, molecular sensors, and functional architectures.

It is well-known that hydrogen-bond interactions do not operate effectively in water because water molecules are constant competitors.[5,6] For this reason, the formation of a complementary hydrogen-bond between nucleobases in water is also ineffective. Accordingly, most of the research on self-assemblies using nucleobase-based polymers were conducted in organic solvents.[7,8] In order to take full advantage of hydrogen-bonds between nucleobases and to obtain stable and predictable nucleobase assemblies in water solution, a rational approach was established to create a hydrophobic micro-environment for nucleobases. In the mid-1990s, Nowick et al. reported that the hydrogen-bond-directed recognition of adenine derivatives occurred within the shielding environment of micelles in aqueous solution.[9,10] However, their micelles in sodium dodecyl sulfate (SDS) aqueous solution were not quite stable with a large critical micelle concentration (CMC) value and sensitivity to ion concentration. In addition, Kim et al. found that incorporated urea-functional groups into block copolymer of poly(ethylene glycol)-block-poly(ethyl-random-urea carbonate) would lower CMC through the hydrogen-bond interaction between urea groups inside the hydrophobic micelle core.[11] Drawing inspiration from these important discoveries, we designed to incorporate nucleobase (T) into the hydrophobic core of a biodegradable amphiphilic copolymer (mPEG-

Received: July 25, 2012
Revised: August 13, 2012
Published: August 14, 2012

b-P(LA-*co*-MPT)) and added complementary alkylated nucleobase (A-C16). Stable hydrogen-bonds inside the core of the nanoparticle (NP) are expected to stabilize the structure of the self-assembled NPs which would be applied as the more suitable drug carriers. We investigated the effect of added A-C16 on the stability and the morphology of their self-assemblies, the effect of pH and temperature variation on the NPs size, and the ability of the NP to encapsulate doxorubiucin (DOX, a model anticancer drug) for potential drug delivery applications. Drug release profiles from DOX-loaded NPs made from block polymers with various A-C16 contents were also studied under different pH values (pH 5.0 and 7.4). Moreover, the cytotoxicity and cellular uptake of the drug-loaded NPs against the MDA-MB-231 cell lines were also evaluated using an MTT assay and confocal laser scanning microscopy (CLSM), respectively.

EXPERIMENTAL SECTION

Materials. The amphiphilic block copolymer mPEG-*b*-P(LA-*co*-MAC), that is, methoxyl poly(ethylene glycol)-*b*-poly(L-lactide-*co*-2-methyl-2-allyloxycarbonyl-propylene carbonate) was prepared according to the literature.[12] 3-Mercapto-1,2-propane-diol (MPD, 95%), bromoacetic acid, 1-bromohexadecane, 2,2-dimethoxy-2-phenylacetophenone (DMPA), adenine (A, 98%), and thymine (T, 99%) were from Aladdin Chemistry Co. Ltd. Shanghai, China. Dicyclohexylcarbodiimide (DCC) and dimethylaminopyridine (DMAP) were from GL Biochem. Ltd. Shanghai, China. Tetrahydrofuran (THF) and toluene were purified by distillation from sodium with benzophenone. *N*,*N*-dimethylformamide (DMF) was dried over calcium hydride for 48 h and then distilled before use. Doxorubicin (DOX) in the form of a hydrochloride salt was purchased from Hisun Pharmaceutical Co., Ltd. Zhejiang, China. 2-(4-Amidinophenyl)-6-indolecarbamidine dihydrochloride (DAPI) and 3-(4,5-dimethylthiazol-2-yl)-2,5-diphenyltetrazolium bromide (MTT) were from Sigma-Aldrich Co. Other reagents were commercially available and used as received.

Measurements. ^{1}H NMR spectra were characterized on a Bruker AV 300 M spectrometer in $CDCl_3$ and DMSO-d_6 at 25 °C. Chemical shifts were given in parts per million with respect to tetramethylsilane (TMS) as an internal reference. Gel permeation chromatography (GPC) measurements were conducted with a Waters 410 GPC equipped with Waters Styragel column (HT3) using $CHCl_3$ as the eluent, and the molecular weights were calibrated with polystyrene standards (molecular weight range, 500 to 3×10^4). FT-IR spectra were recorded on a Bruker Vertex70 Win-IR instrument. Dynamic light scattering (DLS) measurements were performed with a vertically polarized He−Ne laser (DAWN EOS, Wyatt Technology), and the scattering angle was fixed at 90°. Transmission electron microscopy (TEM) studies were performed on a JEM-1011 electron microscope operating at an acceleration voltage of 100 kV. Samples were prepared by drop-casting onto carbon-coated copper grids and then air-dried at room temperature before measurement. The amount of the released DOX was measured using UV−vis spectroscopy (UV-2450PC, Shimadzu) at 480 nm wavelength and calculated on the basis of following calibration curve 1 (pH 7.4) and calibration curve 2 (pH 5.0) using different concentrations of free DOX (0.005−0.1 mg/mL) in the same buffer solution:

$$y = 0.04143 + 7.23615x \quad (R^2 = 0.9967) \tag{1}$$

$$y = 0.06619 + 11.3844x \quad (R^2 = 0.9957) \tag{2}$$

where y is the absorption intensity of DOX, x is the concentration of DOX, and R is the correlation coefficient.

Synthesis of 9-Hexadecyladenine (A-C16). A-C16 was synthesized according to the previous report (Scheme 1).[13] A DMF solution of adenine (1.00 g, 7.4 mmol), 1-bromohexadecane (2.44 g, 8.0 mmol), and anhydrous potassium carbonate (1.08 g, 7.8 mmol) were stirred at 60 °C for 48 h. The resulting insoluble material was washed with water and recrystallized from ethanol. Yield: 90%. ^{1}H NMR (300 MHz, DMSO-d_6, 25 °C, TMS, ppm): δ = 8.11 (d, 2H, CH), 7.16 (s, 2H, NH_2), 4.10 (t, 2H, CH_2), 1.81 (m, 2H, CH_2), 1.24 (m, 26H, CH_2), 0.83 (t, 3H, CH_3).

Scheme 1. Synthesis of Amphiphilic Biodegradable Block Copolymer Bearing Thymine Moieties: mPEG-*b*-P(LA-*co*-MPT) and 9-Hexadecyladenine (A-C16)

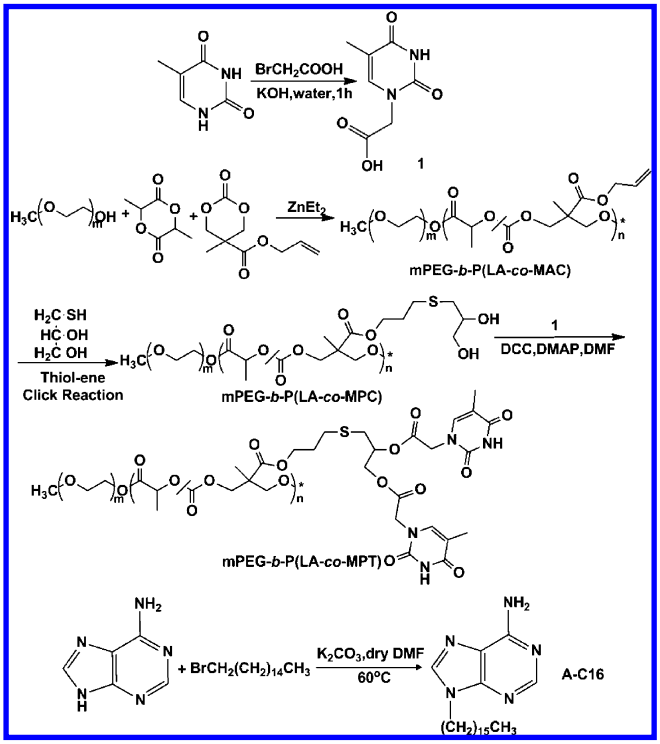

Synthesis of 1-(Carboxymethyl)thymine (T-COOH). T-COOH was synthesized from thymine (Scheme 1) as described in the literature.[14] Thymine (5 g, 39.68 mmol), KOH (11 g, 196.43 mmol), and bromoacetic acid (11 g, 79.71 mmol) were dissolved in water (100 mL) and refluxed for 1 h. The solution was cooled to room temperature, adjusted to a pH to 2. The resulting precipitate was collected by filtration and washed with water, ethanol, and EtOAc to yield the product (12.03 g, 80%) as a white powder. ^{1}H NMR (300 MHz, DMSO-d_6, 25 °C, TMS, ppm): 1.75 (s, 3H, CH_3), 4.36 (s, 2H, CH_2), 7.5 (s, 1H, ArH), 11.36 (s, 1H, NH).

Synthesis of mPEG-*b*-P(LA-*co*-MPC). mPEG-*b*-P(LA-*co*-MPC) was synthesized by the radical thiol−ene addition reactions (Scheme 1).[12] The block copolymer mPEG-*b*-P(LA-*co*-MAC), 3-mercapto-1,2-propanediol (MPD, 5 fold) and DMPA (1 wt %) were dissolved in DMF, followed by 30 min N_2-bubbling to eliminate dissolved oxygen. Then the mixture was stirred at room temperature under UV light (365 nm). After 6 h, the mixture was poured into an excess amount of cold diethyl ether to obtain the mPEG-*b*-P(LA-*co*-MPC) precipitate.

Synthesis of mPEG-*b*-P(LA-*co*-MPT). mPEG-*b*-P(LA-*co*-MPC) (0.4 g, 1.00 mmol of −OH group), T-COOH (0.53 g, 3 mmol), and DMAP (0.18 g, 1.5 mmol) were dissolved in 20 mL of DMF.[15] The mixture was chilled to 0 °C in an ice bath before DCC (3.1 g, 15 mmol) was added. After 24 h, the product was purified by dialysis against methanol over 2 days in a dialysis bag (MWCO = 3500). Then the product was poured into an excess amount of cold diethyl ether to get mPEG-*b*-P(LA-*co*-MPT) precipitate.

Preparation of NPs and Determination of Critical Aggregation Concentration (CAC). Typically, mPEG-*b*-P(LA-*co*-MPT) and A-C16 were dissolved in THF with different molar ratios at room temperature and the mixed solution was added dropwisely into 10 mL of deionized water under stirring. The THF was tardily removed at the ambient temperature over 4 h by rotary evaporation to get the NP solution.

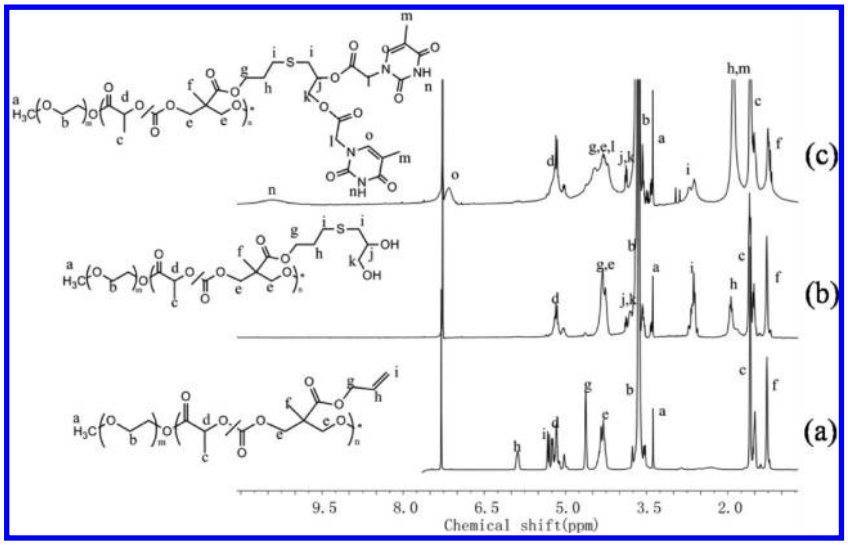

Figure 1. ^{1}H NMR spectra (300 MHz, $CDCl_3$, 25 °C) of (a) mPEG-*b*-P(LA-*co*-MAC), (b) mPEG-*b*-P(LA-*co*-MPC), and (c) mPEG-*b*-P(LA-*co*-MPT).

The CAC was measured using pyrene as a fluorescence probe. Steady state fluorescence spectra were obtained by a Perkin-Elmer LS55 luminescence spectrometer. The NP solutions with various concentrations from 10^{-5} to 1.0 mg/mL were added to a series of volumetric flasks, and the pyrene concentration in the final solution was fixed at 6×10^{-7} mol/L (the saturation solubility of pyrene in water at 22 °C). Then the flasks were thermostatted at 25 °C for about 2 h to equilibrate pyrene partition between water and NPs. The emission wavelength was set at 391 nm for fluorescence excitation spectra. The spectra were recorded at a scan rate of 500 nm/min.

Evaluation of NPs Stability in the Presence of Serum Protein. The NP solutions were mixed with equal volumes of PBS solution (pH 7.4, 0.01 M) containing 10% BSA and incubated at 37 °C.[16] At various time points, 10 mL aliquots of the solutions were removed and analyzed by DLS (n = 3).

Drug Loading into NPs. DOX-loaded NPs were prepared by a dialysis method. Briefly, DOX·HCl (5 mg) and 3 mol of TEA were dissolved in DMSO (1 mL) and added to a THF (2 mL) solution containing mPEG-*b*-P(LA-*co*-MPT) and A-C16. The mixture was added slowly to 10 mL of water and ultrasonicated for 10 min. After being stirred for an additional 2 h, the solution was transferred to a 3500 Da molecular weight cutoff dialysis bag and dialyzed for more than 24 h to get rid of the free DOX and organic solvent. The final solution in the dialysis bag was freeze-dried to give red spongelike micelles. To determine the drug loading content, the DOX-loaded NP was dissolved in DMSO. The UV absorbance at 480 nm was measured to determine the DOX concentration based on the standard calibration curve obtained from free DOX in DMSO.

***In Vitro* DOX Release.** The freeze-dried DOX-loaded NPs were dissolved in phosphate saline buffer (pH 7.4) or acetate buffer (pH 5.0) at a concentration of 1 mg/mL. The above mixture was transferred into a dialysis bag with a molecular weight cutoff of 3500 Da. The bag was then immersed into a container with 20 mL of buffer solution at the same pH value as that inside the bag. The outer phase of the buffer solution was oscillated at 37 °C (90 r/min). At selected time intervals, 1 mL of the external buffer was withdrawn for UV−vis analysis and replaced with the same amount of fresh buffer solution. The released amount of DOX was determined from the absorbance at 480 nm with the help of a calibration curve of DOX in the same buffer. Then the accumulative weight and relative percentage of the released DOX were calculated as a function of incubation time.

Cell Lines. Two cell lines, including L929 (mouse fibroblasts cells) and MDA-MB-231 (human breast cancer cells) were chosen for cell tests. L929 and MDA-MB-231 cells (HTB-26) were supplied by the Medical Department of Jilin University, China. L929, MDA-MB-231 cells were cultured in Dulbecco's modified Eagle's medium (DMEM, GIBCO) supplied with 10% heat-inactivated fetal bovine serum (FBS, GIBCO), 2 mM L-glutamine, 100 U/mL penicillin, and 100 μg/mL streptomycin (Sigma), and the culture medium was replaced once very day.

***In vitro* Cytotoxicity of mPEG-*b*-P(LA-*co*-MPT)/A-C16 NPs.** L929 cells were used to evaluate the biocompatibility of four different types of NPs by MTT assay. The cells were seeded in 96-well plate at a density of 10 000 cells/well in 100 μL of DMEM. Then five concentrations (1.0, 0.5, 0.25, 0.125, and 0.0625 mg/mL) of NPs were added to the wells, and three parallel wells for each sample were used at a specific concentration. After coincubation with L929 cells for 48 h, 20 μL of MTT solution in PBS (5 mg/mL) was added to each well and the plate was incubated for another 4 h at 37 °C. After that, the medium containing MTT was removed, and 150 μL of DMSO was added to each well to dissolve the MTT formazan crystals. Finally, the plates were shaken for 10 min, and the absorbance of formazan product was measured at 492 nm by a microplate reader.

Cellular Uptake Studies. Cellular uptakes by MDA-MB-231 cells were examined using a confocal laser scanning microscope (CLSM). MDA-MB-231 cells were seeded in 6-well culture plates (a sterile coverslip was put in each well) at a density of 1×10^5 cells/well and allowed to adhere for 24 h. Then the cells were treated with free DOX (10 μg/mL) or DOX-loaded mPEG-*b*-P(LA-*co*-MPT)/A-C16 NP (T/A = 1/2, mol/mol; 10 μg/mL equivalent DOX concentration). After incubation for 0.5, 4, or 24 h at 37 °C, the supernatant was carefully removed and the cells were washed three times with ice-cold PBS and fixed with 4% formaldehyde. After the nucleus was stained with DAPI, the slides were mounted and imaged with an Olympus FV1000 confocal laser scanning microscope imaging (CLSM) system (Japan).

Anticancer Activity Analyses. The cytotoxicity of DOX-loaded NPs and free DOX against MDA-MB-231 cells were evaluated *in vitro* by MTT assay. Briefly, MDA-MB-231 cells were seeded into 96-well plates with a density of 6×10^3 cells per well in 100 μL of DMEM and incubated for 24 h. Then 100 μL of DOX-loaded NPs or free DOX in DMEM at various DOX concentrations from 0.01 to 100 μg/mL was added to the culture medium, with the exception of the wells as blank, to which the same volume of DMEM medium was added. And the cells were further cultured for 48 h. Twenty μL of MTT stock solution (5 mg/mL, PBS) was then added to each well. After incubation for additional 4 h, 150 μL DMSO was added to the wells and the plates were shaken for 10 min. The absorbance was measured at 492 nm using a microplate reader. The cell viability was normalized to that of MDA-MB-231 cells only cultured in the DMEM.

Table 1. Characterization of mPEG-*b*-P(LA-*co*-MAC) and mPEG-*b*-P(LA-*co*-MPT)

polymer[a]	T^d (number)	$M_n{}^b$ (^{1}H NMR)	$M_n{}^c$ (GPC)	$M_w{}^c$ (GPC)	PDI^c (GPC)
$mPEG_{113}$ -*b*-P(LA_{19} -*co*-MAC_{12})	0	1.01×10^4	1.44×10^4	1.82×10^4	1.26
mPEG-*b*-P(LA-*co*-MPT)	21	1.53×10^4			

[a]Subscript refers to the degree of polymerization of each block. [b]Determined by ^{1}H NMR. [c]Determined by GPC using $CHCl_3$ as the eluent. [d]Determined by UV−vis spectrum and ^{1}H NMR.

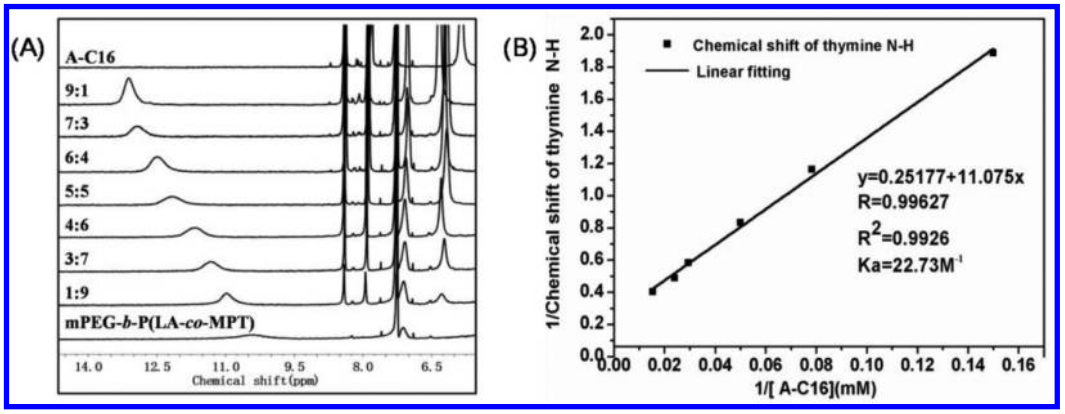

Figure 2. ^{1}H NMR spectroscopic titration. Amide region of the mPEG-*b*-P(LA-*co*-MPT) after the addition of A-C16 was enlarged. The ratios in the figure represent the molar ratios of A/T (A) and Benesi−Hildebrand plots for mPEG-*b*-P(LA-*co*-MPT)/A-C16 association in $CDCl_3$ at 25 °C (B).

RESULTS AND DISCUSSION

Binding Nuleobases with Amphiphilic Copolymers. In order to create a hydrophobic microenvironment for the hydrogen bonding between nucleobases (A and T), an amphiphilic biodegradable copolymer was synthesized and nucleobase (T) was grafted to the hydrophobic segment. These nucleobase-grafted amphiphilic copolymers can self-assemble into NPs, and the hydrogen bonding inside the hydrophobic cores could be well protected from water and expected to be more effective and stable.

For this purpose, T-COOH was first prepared through the reaction of thymine with bromoacetic acid in the presence of potassium hydroxide. The structure of T-COOH was confirmed by ^{1}H NMR spectra (Figure S1 in the Supporting Information). The chemical shifts at 4.4 and 13.2 ppm were assigned to the protons of CH_2 ($-CH_2N-$) and COOH ($-CH_2COOH$) connected with thymine, respectively. mPEG-*b*-P(LA-*co*-MAC) copolymer was synthesized by ROP of L-Lactide (LA) and 2-methyl-2-(allyloxycarbonyl)propylene carbonate (MAC) using mPEG (5000 Da) as a macroinitiator and characterized using ^{1}H NMR and GPC (Scheme 1, Figure 1a, Figure S2 in the Supporting Information, and Table 1). ^{1}H NMR spectra also proved that the allyl group was intact (signals at 4.6, 5.25−5.35, and 5.85−5.95 ppm) during polymerization (Figure 1a). Under UV irradiation and photoinitiator DMPA, mPEG-*b*-P(LA-*co*-MAC) was further modified to mPEG-*b*-P(LA-*co*-MPC) by the radical thiol−ene reaction with MPD as the spacer to provide tailed hydroxyl groups on the side chain for future conjugation with nucleobase (Scheme 1). As shown in Figure 1b, resonances at 4.6 ppm which are attributed to the methylene adjacent to the vinyl group all shifted to 3.4 ppm after the reaction with MPD. Disappearance of the vinyl peaks (resonances at 5.25−5.35 ppm and 5.85−5.95 ppm) and appearance of the new peaks at 1.9 and 2.6 ppm indicated complete consumption of the starting material and formation of the corresponding mPEG-*b*-P(LA-*co*-MPC).

mPEG-*b*-P(LA-*co*-MPT) was finally obtained through the condensation reaction between mPEG-*b*-P(LA-*co*-MPC) and T-COOH (Scheme 1). As shown in the ^{1}H NMR spectra, the characteristic peaks of thymine derivative appeared at 1.89, 7.16, and 10.42 ppm (Figure 1c). In addition, ^{1}H NMR spectra of mPEG-*b*-P(LA-*co*-MPT) in DMSO-d_6 (Figure S3 in the Supporting Information) also illustrated the successful synthesis. The grafting numbers of thymine on copolymer were calculated from the integration ratio of peaks at 3.5 ppm (the $-CH_2-$ of mPEG) and 1.89 ppm (the $-CH_3$ of thymine). The conjugation degree of thymine can also be obtained by comparison with the UV absorbance of the copolymer at 274 nm with the standard calibration curve obtained from free T-COOH in DMF, which is consistent with ^{1}H NMR results. These results showed that the number of thymine grafts on the copolymer was 21 (Table 1) and the grafting efficiency was 87.5%.

Hydrogen Bonding Interactions between mPEG-*b*-P(LA-*co*-MPT) and A-C16. As the complementary molecule of thymine, adenine was modified with 1-bromohexadecane to obtain A-C16 (Scheme 1). The long alkyl chain (C16) provided enhanced oil-solubility to adenine, making it possible to form hydrogen-bonding with the grafted thymine in the hydrophobic core. The ^{1}H NMR signals at 4.10, 1.81, 1.24, and 0.83 ppm clearly confirmed the successful synthesis of A-C16 (Figure S4 in the Supporting Information).

The formation of complementary hydrogen bonds between mPEG-*b*-P(LA-*co*-MPT) and A-C16 was first analyzed by ^{1}H NMR titration experiment in organic solution ($CDCl_3$) as reported.[13] The resonance of N−H proton of the grafted thymine kept shifting to high field with the increase of the concentration of added A-C16 (Figure 2A). The change in chemical shift was proved to be induced by the fast exchange between associated and dissociated A−T complex.[17] The Benesi−Hildebrand model, which is a mathematical method for determining the association constant (K_a) from a NMR titration experiment, was performed to fit the nonlinear chemical shift data as expected for a dimeric hydrogen-bond

association with the assumption that the complex is formed in 1:1 stoichiometry using the following equation:[18]

$$\frac{1}{\Delta\delta} = \frac{1}{K_a \Delta\delta_{max}[\text{A-C16}]} + \frac{1}{\Delta\delta_{max}}$$

where $\Delta\delta_{max}$ is the maximum change of the chemical shift of the thymine NH proton. A double-reciprocal plot based on the association of the A−T complex possesses a linear relationship as shown in Figure 2B. The K_a, which was calculated from the slope of the plot, was 22.73 M^{-1}, which is consistent with K_a values reported previously for adenine−thymine base pair recognition (~10−100 M^{-1} in $CDCl_3$).

The hydrogen bonding interactions between mPEG-*b*-P(LA-*co*-MPT) and A-C16 in the bulk state were also examined using FT-IR spectroscopy (Figure S5 in the Supporting Information). The results showed that the C═O stretching peaks between 1725−1625 cm^{-1} became broader with the addition of A-C16 and shifted to lower frequency, indicating an existence of complementary hydrogen-bonds between mPEG-*b*-P(LA-*co*-MPT) and A-C16 complexes.[19]

Effect of the Hydrogen Bonding on the Self-Assembly of Amphiphilic Copolymer in Aqueous Solution. Besides the core or shell cross-linking, stabilized noncovalent interaction is one of the important efforts to enhance NP stability. These noncovalent interactions act as the collective driving force to the formation of stable aggregates.[11] In our designation, both adenine and the grafted thymine are located inside the cores of the NPs which are formed by the mPEG-*b*-P(LA-*co*-MPT) copolymers. Since A-C16 could form the hydrogen-bonds with the grafted thymine on mPEG-*b*-P(LA-*co*-MPT) in organic solution, which was proved from the above experiments, the hydrophobic microenvironment provided by the NP cores would ensure the base pair to form stable hydrogen-bonds inside NPs, making it possible to obtain a more stable NP structure in aqueous solution.

The first result about the change of CAC seemed to be quite coincident with our assumption. The addition of A-C16 significantly decreased the CAC of NPs, implying the more stable NP structure than that of the blank NP without adding any A-C16. When the molar ratio between T and A was 1:1, the NPs possessed the lowest CAC value (1.2 mg/L) (Table 2). However, it is still too early to draw the conclusion that the stabilization effect on NPs is coming from the hydrogen bonding between the encapsulated adenine and the grafted thymine. It is acknowledged that to increase the content of the hydrophobic segment in the amphiphilic copolymer would also decrease the CAC value of the resulted NPs of increased size. Since A-C16 possesses the long alkyl chain, the effect on the CAC value by the addition of the hydrophobic C16 segment could not be ignored. To clarify the effect, we synthesized another series of NPs using mPEG-*b*-P(LA-*co*-MPT) copolymer mixed with 1-bromohexadecane without adenine modification. Apparently, the existence of C16 segment is conducive to the size increasing of the NPs (data not shown), since the hydrophobic content was higher than that of the blank copolymer NPs. However, a slight decrease of CAC values (3.2, 3.0, 2.9 mg/L, respectively) was observed while the same ratios of C16 as A-C16 to T were encapsulated. The CAC changes in the C16 added systems were much smaller than that in the A-C16 added ones. These results indicated that the hydrogen bonding interactions between mPEG-*b*-P(LA-*co*-MPT) and A-C16, rather than the simple hydrophobic interactions, played a more important role of stabilizing the NP structure with a decreased CAC value in the aqueous environment.

The size and morphology change of mPEG-*b*-P(LA-*co*-MPT)/A-C16 NPs were also characterized by DLS and TEM measurements. Apparently, the addition of A-C16 increased the average diameter of the NPs (Table 2). Different morphologies of NPs could be observed by changing the ratio between mPEG-*b*-P(LA-*co*-MPT) and A-C16 (Figure 3). When the molar ratio of the grafted T to A was 1:0.5, the micelle structure formed by the blank copolymer was changed to vesicle (Figure 3a, b). When the ratio was 1:1, the spherical micellar structure again appeared (Figure 3c). After increasing the A-C16 content to a molar ratio of 1:2, the morphology of the aggregates transferred to vesicles again (Figure 3d). It is well-known that several factors would affect the morphologies of amphiphilic copolymer assembly in aqueous solution, such as the chain interaction in the core, the degree of core-chain stretching, and

Table 2. Properties of the mPEG-*b*-P(LA-*co*-MPT)/A-C16 Micelles

polymer[a]	CMC[c] (mg/L)	diameter[d] (nm)	PDI[d]	drug loading[e] (wt %)
$mPEG_{113}$ -*b*-P(LA_{19} -*co*-MPT_{21})/A-C_{16} (1:0)[b]	3.7	55	0.089	8.78
$mPEG_{113}$ -*b*-P(LA_{19} -*co*-MPT_{21})/A-C_{16} (1:0.5)[b]	2.2	155	0.076	8.16
$mPEG_{113}$ -*b*-P(LA_{19} -*co*-MPT_{21})/A-C_{16} (1:1)[b]	1.2	172	0.085	9.35
$mPEG_{113}$ -*b*-P(LA_{19} -*co*-MPT_{21})/A-C_{16} (1:2)[b]	1.7	187	0.07	9.79

[a]Subscript refers to the degree of polymerization of each block determined by ^1H NMR. [b]Numbers in parentheses are the mole ratios of T and A. [c]Determined by fluorescence spectrometer. [d]Diameter and polydispersity index (PDI) of micelles were determined by DLS. [e]Measured with UV−visible spectroscopy.

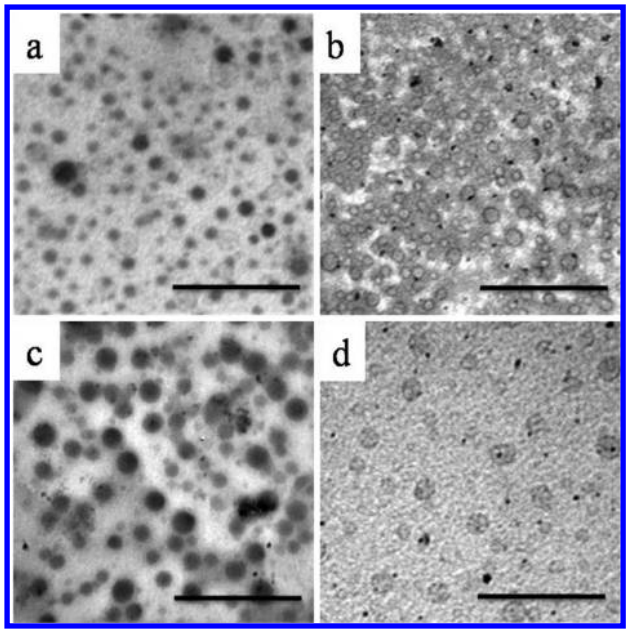

Figure 3. TEM pictures of (a) pure mPEG-*b*-P(LA-*co*-MPT) and the mixtures of mPEG-*b*-P(LA-*co*-MPT) and A-C16 at T/A (mol/mol) of (b) 1/0.5, (c) 1/1, and (d) 1/2. Bar = 500 nm.

the core−shell interfacial energy.[20−22] In our case, A-C16 has two main functions, i.e., to form strong hydrogen bonding interaction using A with T on copolymers and to increase the hydrophobic content by C16 to enlarge the core size. The addition of small amount of the long hydrophobic-tailed A-C16 (T/A = 1:0.5, mol/mol) could not only reduce the chain interaction by providing more space between the core-chains but also change the hydrophobic core to larger size. Therefore, the vesicle morphology would be the most favorable to maintain the assembly structure. At the same time, the chain stretching of mPEG-*b*-P(LA-*co*-MPT) increased in response to the increase of the core diameter. The chain stretching induced entropic penalty was relieved by addition of more amount of A-C16 (like T/A = 1:1, mol/mol), and the micellar morphology was formed due to the increased electron density in the core. By further addition of A-C16 (like T/A = 1:2, mol/mol), the excess amount of the A-C16 that did not participate in the formation of hydrogen-bonds would accumulate in the inner domain of the NP to obtain the vesicular aggregates.[20,23]

Reportedly, the hydrogen-bond is utterly sensitive to the environmental changes (such as temperature and pH), for example, Wang et al investigated the influence of temperature and pH on micelles of PCL-A:U-PEG formed based on multiple hydrogen bonding interactions between PCL-A and PEG-U.[24] For this reason, we also applied experiments to investigate the effect of temperature and pH on the NP stability. First, turbidometry was performed to determine the effect of temperature on the hydrogen bonding interactions between mPEG-*b*-P(LA-*co*-MPT) and A-C16. NP aqueous solution was gradually heated in a sealed vessel from 25 to 80 °C. Relative absorbance at 700 nm was monitored after that. As expected, all the NPs were stable at room temperature. The mPEG-*b*-P(LA-*co*-MPT) NP without A-C16 was stable to the temperature change, since there was no turbidity change observed. When A-C16 was involved in the NP system, the increasing of the solution turbidity was observed as the temperature elevated. More A-C16 was added, and more of a sharp increase of the solution turbidity could be identified, until the grafted T was saturated by the hydrogen-bonds with A-C16 (Figure 4). The results implied that the hydrogen-bonds between the copolymers and A-C16 were gradually dissociated by increasing temperature. Without the hydrogen bonding stabilization, these large-sized (more than 150 nm) NPs structure became unstable and would be destroyed to form unordered aggregates to increase the solution turbidity.[25]

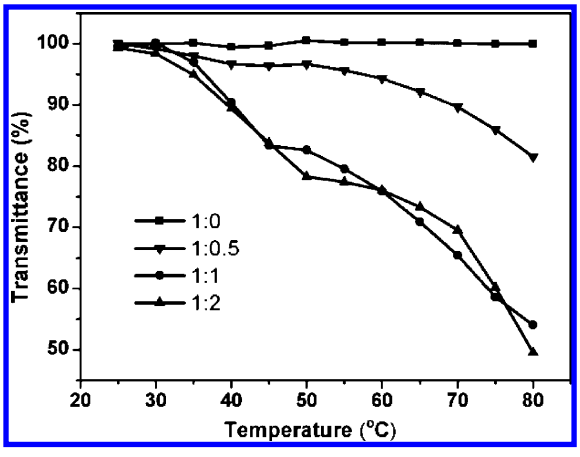

Figure 4. Turbidity change of mPEG-*b*-P(LA-*co*-MPT)/A-C16 micelles at different mole ratios of T/A.

Similar results could be obtained by checking the effect of temperature on the size of NPs using DLS measurements. Four NPs solutions (0.5 mg/mL) in PBS (pH 7.4) were first prepared. Then the size of the NPs was determined by DLS at different temperatures. Figure 5a showed that the size of the blank NP had little change with temperature. When A-C16 was added, the average diameter varied greatly from room temperature to 45 °C. It is supposed that the dissociation of complementary hydrogen bonding between A and T happened at higher temperature and smaller sized aggregates would be entropically favored over larger ones.[26] When the temperature was further increased to 60 °C, these small-sized aggregates would gather into large particles, which were in accordance with the previous turbidometry studies (Figure 5b−d). These results also implied that the mPEG-*b*-P(LA-*co*-MPT)/A-C16 NPs system would have the possibility to be utilized in the human body as therapeutic delivery, since the NPs had suitable stability at physiological temperature (37 °C).

Second, to evaluate the effect of pH on hydrogen-bonds, the NPs solutions (10 mL) were mixed with acetate buffer solution (5 mL, pH 5.0) at 25 °C for 1, 4, and 24 h. Then the size changes of four NPs in acetate buffer were monitored with DLS. As seen in Figure S6 in the Supporting Information, all the NP sizes increased gradually no matter if A-C16 was added or not, which can be ascribed to two possibilities. First, the protonation of the nitrogen atoms in nucleobases increased the compulsive force between the hydrophobic segments, resulting in a much looser core of the NPs. Second, the swell of the polyester segment of the copolymer in acid condition would also increase the NPs size.

In addition, the stability of the NP was studied in PBS containing 10% FBS at 37 °C by monitoring the particle size change as a function of time. As it is observed in Figure 6, there was no significant change in size over 48 h, indicating that neither aggregation nor destabilization was induced by serum proteins.

***In Vitro* Cytotoxicity of mPEG-*b*-P(LA-*co*-MPT)/A-C16 NPs.** In order to evaluate the cytotoxicity of the materials, cellular biocompatibility experiments on mPEG-*b*-P(LA-*co*-MPT)/A-C16 (T/A = 1:0, 1:0.5, 1:1, 1:2) NPs were carried out using the MTT method with L929 as the test cell line. Figure S7 in the Supporting Information shows the cell viability after 48 h incubation with the NPs at different concentrations. The results demonstrate that no obvious cytotoxicity against L929 cells is observed even if the concentration of copolymer NPs is up to 1 mg/mL, indicating high safety of these NPs.

Drug Loading and Release *in Vitro*. To assess the influence of hydrogen bonding on drug incorporation, DOX was used as a model anticancer drug to evaluate the drug loading and release properties. The drug loading contents (DLC) for DOX-loaded NPs were around 8−10% (Table 2). Although the carbonyl groups, hydroxyl groups, and primary amine group in DOX molecule could act as H-bonding sites with the nucleobases,[11] there was no significant difference on DLC between different kinds of NPs.

The *in vitro* DOX release from the NPs was conducted in two different buffered solutions (pH 7.4 and 5.0) at 37 °C. As shown in Figure 7A, the burst release of DOX from the blank NPs (T/A = 1/0) was well constrained by the addition of A-C16. Besides, the more A-C16 involved, the slower the drug release from the mPEG-*b*-P(LA-*co*-MPT)/A-C16 NPs at pH

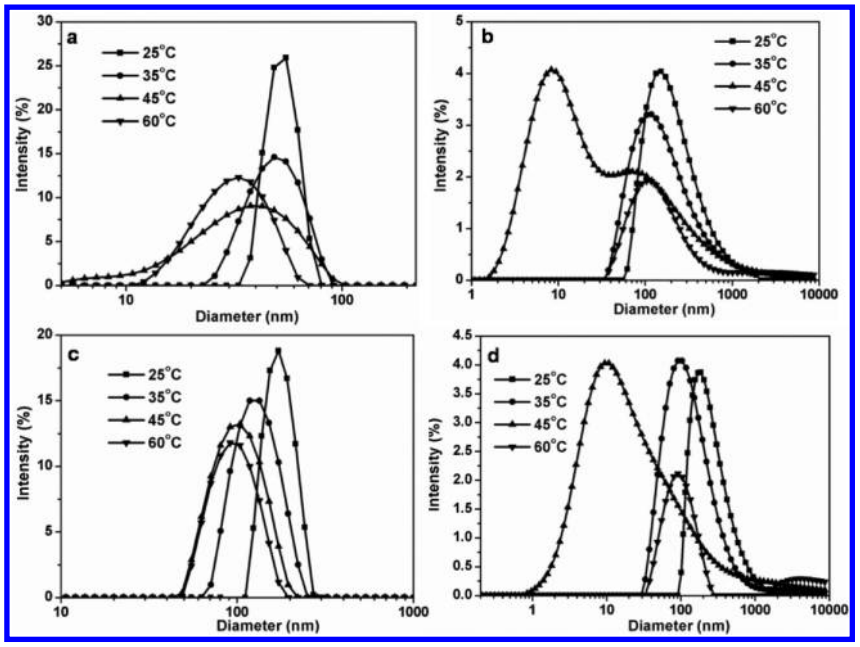

Figure 5. Size distribution change of mPEG-*b*-P(LA-*co*-MPT)/A-C16 NPs at different temperatures determined by DLS: (a) T/A = 1/0, (b) T/A = 1/0.5, (c) T/A = 1/1, and (d) T/A = 1/2.

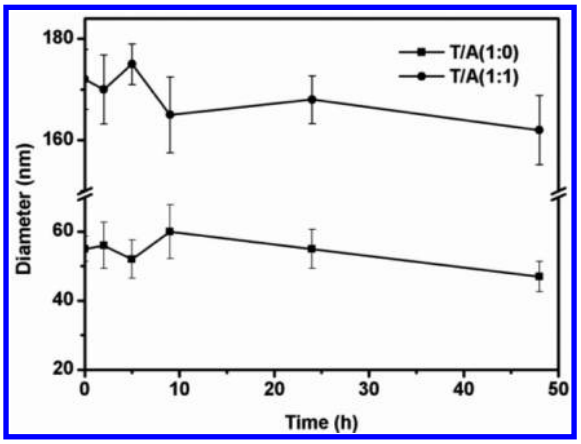

Figure 6. Particle size of micelles in the presence of 10% FBS in PBS (pH 7.4) at 37 °C for different time periods determined by DLS (the results are presented as a mean of three replications and standard deviation).

7.4. The strong hydrogen bonding interaction to stabilize the NP structure and the attractive interaction between DOX molecules and A-C16 would be the main reason for this retarded release behavior. At the same time, DOX release became much faster at pH 5 (Figure 7B). The better solubility of DOX at pH 5.0 and the protonation effect which destroyed the multiple complementary hydrogen-bonds between nucleobases would have the contribution to the fast drug release. However, the drug release trend was completely opposite to that at pH 7.4. At pH 5.0, the more A-C16 involved, the much faster drug release from the mPEG-*b*-P(LA-*co*-MPT)/A-C16 NPs. It should be noted that A-C16 and DOX were all protonized at pH 5.0. When more amount of A-C16 was encapsulated into the NP, the repulsion force between the positive-charged A-C16 and DOX would become stronger, leading to the rapid and larger release of DOX. Among these NP systems, the mPEG-*b*-P(LA-co-MPT)/A-C16 NP with a T/A ratio of 1/2 demonstrated the best pH-sensitivity (lowest drug release at pH 7.4 and highest drug release at pH 5.0). This character would be fairly useful for drug delivery to obtain a

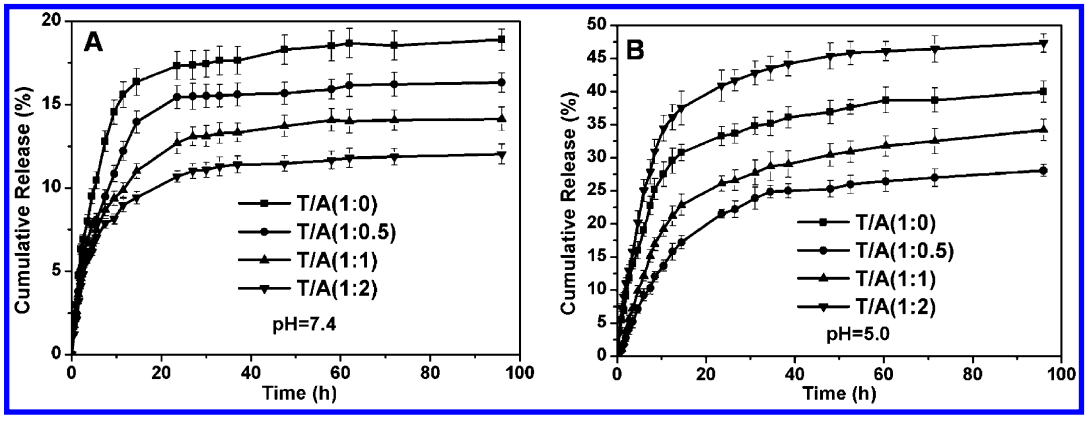

Figure 7. *In vitro* release profiles of doxorubicin (DOX) from mPEG-*b*-P(LA-*co*-MPT)/A-C16 micelles at pH 7.4 (A) and pH 5.0 (B) at 37 °C. Each data point represented the mean ± SD (n = 3).

long-term circulation in blood and an effective drug release at the tumor site, since the microenvironment around the tumor cells and inside the endosome is acidic.

Cell Internalization. The cellular uptake and intracellular release behaviors of free DOX and DOX-loaded mPEG-*b*-P(LA-*co*-MPT)/A-C16 (T/A = 1/2) NP were investigated by CLSM. Free DOX and DOX-loaded NP were incubated with MDA-MB-231 cells at 37 °C for 0.5, 4, and 24 h, respectively. As shown in Figure 8, intracellular distribution of the DOX-loaded NP is different from that of free DOX. After 0.5 h of cell incubation with the free DOX, strong fluorescence was observed in the cell nuclei (Figure 8A). In contrast, DOX fluorescence was observed only in the cytoplasm rather than the cell nuclei, when cells were incubated with the DOX-loaded NP for 0.5 h (Figure 8D). When the cells were exposed to free DOX for 4 h, more intense DOX-fluorescence was observed in the nuclei (Figure 8B). In contrast, the cells incubated with DOX-loaded NP for 4 h emitted significantly increased fluorescence in cell nuclei in addition to the very weak fluorescence in cytoplasm (Figure 8E). When the incubation period increased to 24 h, cell deformation was observed when treated with free DOX (Figure 8C). For DOX-loaded NP, the red fluorescence nuclei increased with time (Figure 8F). These data not only demonstrate that mPEG-*b*-P(LA-*co*-MPT)/A-C16 NP is an efficient vehicle to transport DOX into the cytoplasm but also suggest that the internalization mechanism of NP is different from that of free DOX. Similar results were reported by Xin tao Shuai and co-workers in the MCF-7 cell incubation with MPEG5k-b-PCL24.7k micelles.[27] Moreover, Kataoka et al. reported the same results in the SBC-3 cell incubation with PEG-P(Asp-Hyd-DOX) micelle. In their study, dot-shaped fluorescence was observed within cytoplasm and was considered to be micelles trapped in the endocytic vesicles.[28] As observed in Figure 8D,E, DOX fluorescence of the cytoplasm was mainly in punctuated dot-shape, which suggested that DOX-loaded micelles were internalized through an endocytosis pathway and were then localized in acidic endocytic compartments (i.e., endosomes and later lysosomes). Because the *in vitro* DOX-release from the NP was a relatively slow process even at pH 5 (Figure 7), the DOX transported by these micelles will not enter the nuclei as quickly as the free DOX, as indicated by the CLSM measurement. DOX transported by NP will eventually enter the nuclei where DOX interacts with topoisomerase II to cause DNA cleavage and cytotoxicity,[29] as the following cytotoxicity results demonstrate that the growth of MDA-MB-231 cells can be effectively inhibited.

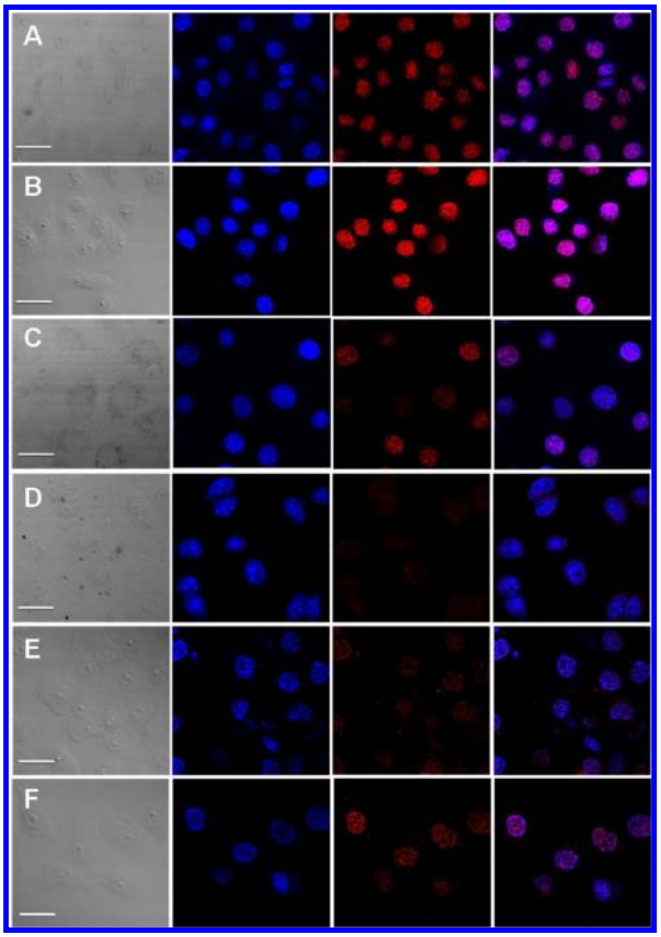

Figure 8. CLSM-images of MDA-MB-231 cells incubated with free DOX for 0.5 (A), 4 (B), and 24 h (C) and with DOX-loaded mPEG-*b*-P(LA-*co*-MPT)/A-C16 (T/A = 1/2) NP for 0.5 (D), 4 (E), and 24 h (F). For each row, images from left to right were the cells with bright field, with nucleus stained with DAPI (blue), with DOX (red) fluorescence, and overlaid images. Bar = 30 μm.

***In vitro* Cytotoxicity of Drug-Loaded NPs.** The *in vitro* cytotoxicities of DOX-loaded NPs and the free DOX were evaluated by MTT assay against MDA-MB-231 cancer cells with different DOX dosages from 0.001 to 100 μg/mL. As shown in Figure 9, the half maximal inhibitory concentration (IC_{50}) values for free DOX and DOX-loaded NPs (T/A = 0/1, 0.5/1, 1/1, 2/1) against MDA-MB-231 cell lines were 0.87, 4.16, 4.89, 3.21, and 2.72 μg/mL, respectively. These results first demonstrated that DOX-loaded NPs were able to enter the cells and exhibited a suitable pharmacological effect on cancer cells. Besides, free DOX showed higher inhibition for cancer cell proliferation than that of the DOX-loaded NPs, which has been proved in the previous literature.[27,30,31] The lower cytotoxicity of DOX-loaded NPs can be attributed to the slow release of DOX from NPs as evidenced by the *in vitro* release profiles in Figure 7 and delayed nuclear uptake in MDA-MB-231 cells which has been proved by internalization studies by CLSM (Figure 8).

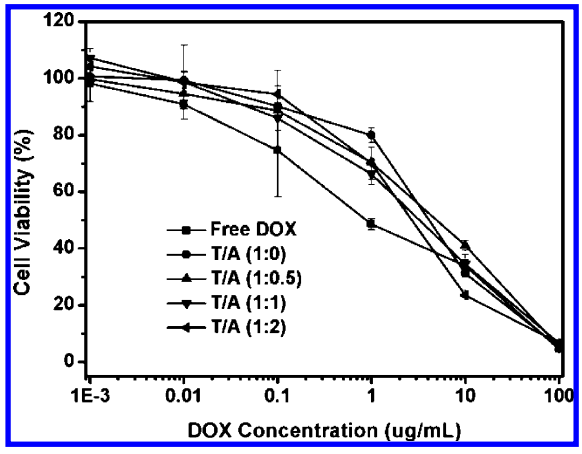

Figure 9. Cell viability of MDA-MB-231 cells against DOX-loaded mPEG-*b*-P(LA-*co*-MPT)/A-C16 micelles at different mole ratios of A and T after cultured for 48 h with different DOX dosages.

CONCLUSIONS

The present study highlighted the important role of the hydrophobic core of the amphiphilic NPs which provided a microenvironment for the nucleobases (A and T) and protected the hydrogen bonding effectively and the importance of the hydrogen bonding of nucleobases in stabilizing NPs for drug delivery. We synthesized amphiphilic biodegradable copolymer mPEG-*b*-P(LA-*co*-MPT) containing the nucleobase thymine. The addition of A-C16 can significantly lower the CAC of block copolymers and enhance stability of the NPs in aqueous solution. Different morphologies of assembly could be observed by changing the molar ratio of T and A. Besides, the addition of A-C16 could also adjust the drug release rate. What's more, the resulting copolymer and NPs showed high biocompatibility, and the DOX-loaded NPs could be successfully internalized to kill cancer cells efficiently.

ASSOCIATED CONTENT

Supporting Information

^{1}H NMR spectra of T-COOH in DMSO-d_6 (Figure S1), GPC curve of mPEG-*b*-P(LA-*co*-MAC) (Figure S2), ^{1}H NMR spectra of mPEG-*b*-P(LA-*co*-MPT) (Figure S3) and A-C16 (Figure S4) in DMSO-d_6, FT-IR spectra in the range of 1725−1625 cm^{-1} for mPEG-*b*-P(LA-*co*-MPT) in the bulk state in the presence of different contents of A-C16 (Figure S5), size change of mPEG-*b*-P(LA-*co*-MPT)/A-C16 NPs at pH 5.0 (25 °C) monitored by DLS (Figure S6), and *in vitro* cytotoxicities of mPEG-*b*-P(LA-*co*-MPT)/A-C16 micelles (Figure S7). This material is available free of charge via the Internet at http://pubs.acs.org.

AUTHOR INFORMATION

Corresponding Author

*Yubin Huang: phone/fax, +86-431-85262769; e-mail, ybhuang@ciac.jl.cn. Fanbo Meng: phone, +86-13159757035; e-mail, mengfb@jlu.edu.cn.

Notes

The authors declare no competing financial interest.

ACKNOWLEDGMENTS

The authors would like to thank the financial support from the National Natural Science Foundation of China (Grants Nos. 51021003 and 21174143), the Ministry of Science and Technology of China (973 Project, Grant No. 2009CB930102; 863 Project, Grant No. SS2012AA020603), "100 Talents Program" of the Chinese Academy of Sciences (Grant No. KGCX2-YW-802), and the Jilin Provincial Science and Technology Department (Grant No. 20100588).

REFERENCES

(1) Sivakova, S.; Rowan, S. J. *Chem. Soc. Rev.* **2005**, *34*, 9−21.
(2) Wilson, A. J. *Soft Matter* **2007**, *3*, 409−425.
(3) Watson, J. D.; Crick, F. H. *Nature* **1953**, *171*, 737−738.
(4) Sessler, J. L.; Lawrence, C. M.; Jayawickramarajah, J. *Chem. Soc. Rev.* **2007**, *36*, 314−325.
(5) Araki, K.; Yoshikawa, I. *Top. Curr. Chem.* **2005**, *256*, 133−165.
(6) Sawada, T.; Fujita, M. *J. Am. Chem. Soc.* **2010**, *132*, 7194−7201.
(7) Lin, I. H.; Cheng, C.-C.; Yen, Y.-C.; Chang, F.-C. *Macromolecules* **2010**, *43*, 1245−1252.
(8) Lo, P. K.; Sleiman, H. F. *Macromolecules* **2008**, *41*, 5590−5603.
(9) Nowick, J. S.; Chen, J. S. *J. Am. Chem. Soc.* **1992**, *114*, 1107−1108.
(10) Nowick, J. S.; Chen, J. S.; Noronha, G. *J. Am. Chem. Soc.* **1993**, *115*, 7636−7644.
(11) Kim, S. H.; Tan, J. P. K.; Nederberg, F.; Fukushima, K.; Colson, J.; Yang, C.; Nelson, A.; Yang, Y.-Y.; Hedrick, J. L. *Biomaterials* **2010**, *31*, 8063−8071.
(12) Yue, J.; Li, X.; Mo, G.; Wang, R.; Huang, Y.; Jing, X. *Macromolecules* **2010**, *43*, 9645−9654.
(13) Cheng, C. C.; Huang, C. F.; Yen, Y. C.; Chang, F. C. *J. Polym. Sci., Part A: Polym. Chem.* **2008**, *46*, 6416−6424.
(14) Song, Q.-H.; Wang, H.-B.; Tang, W.-J.; Guo, Q.-X.; Yu, S.-Q. *Org. Biomol. Chem.* **2006**, *4*, 291−298.
(15) Zhou, J.; Li, Z.; Liu, G. *Macromolecules* **2002**, *35*, 3690−3696.
(16) Liu, J.; Zahedi, P.; Zeng, F.; Allen, C. *J. Pharm. Sci.* **2008**, *97*, 3274−3290.
(17) Ladmiral, V.; Mantovani, G.; Clarkson, G. J.; Cauet, S.; Irwin, J. L.; Haddleton, D. M. *J. Am. Chem. Soc.* **2006**, *128*, 4823−4830.
(18) Fielding, L. *Tetrahedron* **2000**, *56*, 6151−6170.
(19) Dong, A. J.; Wan, T.; Feng, S. Y.; Sun, D. X. *J. Polym. Sci., Part B: Polym. Phys* **1999**, *37*, 2642−2650.
(20) Chen, S.-C.; Kuo, S.-W.; Chang, F.-C. *Langmuir* **2011**, *27*, 10197−10205.
(21) Chen, Z. Y.; Hua, Z. D.; Xu, L.; Huang, Y.; Zhao, M. P.; Li, Y. Z. *J. Mol. Recognit.* **2008**, *21*, 71−77.
(22) Tung, P.-H.; Kuo, S.-W.; Chen, S.-C.; Lin, C.-L.; Chang, F.-C. *Polymer* **2007**, *48*, 3192−3200.
(23) Chen, S.-C.; Kuo, S.-W.; Liao, C.-S.; Chang, F.-C. *Macromolecules* **2008**, *41*, 8865−8876.
(24) Wang, D.; Su, Y.; Jin, C.; Zhu, B.; Pang, Y.; Zhu, L.; Liu, J.; Tu, C.; Yan, D.; Zhu, X. *Biomacromolecules* **2011**, *12*, 1370−1379.
(25) Uzun, O.; Sanyal, A.; Nakade, H.; Thibault, R. J.; Rotello, V. M. *J. Am. Chem. Soc.* **2004**, *126*, 14773−14777.
(26) Israelachvili, J. N.; Mitchell, D. J.; Ninham, B. W. *Biochim. Biophys. Acta: Biomembranes* **1977**, *470*, 185−201.
(27) Shuai, X.; Ai, H.; Nasongkla, N.; Kim, S.; Gao, J. *J. Controlled Release* **2004**, *98*, 415−426.
(28) Bae, Y.; Fukushima, S.; Harada, A.; Kataoka, K. *Angew. Chem., Int. Ed.* **2003**, *42*, 4640−4643.
(29) Zunino, F.; Capranico, G. *Anti-Cancer Drug Des.* **1990**, *5*, 307−317.
(30) Zhang, W.; Li, Y.; Liu, L.; Sun, Q.; Shuai, X.; Zhu, W.; Chen, Y. *Biomacromolecules* **2010**, *11*, 1331−1338.
(31) Li, Y. L.; Zhu, L.; Liu, Z.; Cheng, R.; Meng, F.; Cui, J. H.; Ji, S. J.; Zhong, Z. *Angew. Chem., Int. Ed.* **2009**, *48*, 9914−9918.